Logarithmic behavior of wall-attached structures in a turbulent boundary layer

Jinyul HWANG and Hyung Jin SUNG†

Department of Mechanical Engineering, KAIST, 291, Yuseong-gu, Daejeon 34141, KOREA

†Corresponding Author: Hyung Jin Sung, hjsung@kaist.ac.kr

ABSTRACT

Wall turbulence is a ubiquitous phenomenon in nature and engineering applications, yet predicting such turbulence is difficult due to its complexity. High-Reynolds-number turbulence, which includes most practical flows, is particularly complicated because of its wide range of scales. Although the attached-eddy hypothesis postulated by Townsend can be used to predict turbulence intensities and serves as a unified theory for the asymptotic behaviors of turbulence, the presence of attached structures has not been confirmed. Here, we demonstrate the logarithmic region of the turbulent intensity by identifying wall-attached structures of streamwise velocity fluctuations through direct numerical simulation of a moderate-Reynolds-number boundary layer. The wall-attached structures are self-similar and composed of multiple uniform momentum zones. The population density of the structures scales inversely with their height, which is reminiscent of the hierarchy of attached eddies. These findings suggest that the identified structures are prime candidates for Townsend's attached-eddy hypothesis and serve as conerstones for understanding the multiscale phenomena of high-Reynolds-number boundary layers.

INTRODUCTION

Understanding wall-bounded turbulent flows is a long-standing challenge because of their complex and chaotic nature. The presence of a wall not only induces the formation of a thin shear layer close to the wall known as the turbulent boundary layer (TBL), where most of the energy consumption occurs in modern vehicles and pipelines but also separates the TBL into different layers composed of multiscale fluid motions. These multiscale phenomena can be characterized in terms of the friction Reynolds number ($Re_\tau = \delta u_\tau/\nu$), which is the ratio of the viscous length scale ν/u_τ (ν is the kinematic viscosity, and u_τ is the friction velocity) and the flow thickness δ. Although much progress has been achieved in characterizing the onset of turbulence and fully turbulent flows at low Re_τ, little progress has been made in the case of high Re_τ turbulence [1], which arises in engineering devices and atmospheric winds ($Re_\tau = O(10^{4–6})$), due to the wide range of scales that govern the transport of mass, momentum and heat.

To elucidate these multiscale phenomena, one approach is to examine the organized motions that retain their spatial coherence for relatively long periods, known as eddies or coherent structures, because these structures are responsible for the dynamical mechanisms and turbulence statistics [2]. Above the buffer layer, the coherent structures are larger and more complex due to the presence of various scales. In this region, the mean streamwise velocity ($\overline{U}$) follows a logarithmic profile along the wall-normal distance y [3]:

$$\overline{U}^+ = \kappa^{-1}\ln(y^+) + A, \tag{1}$$

where $\overline{U}^+ = \overline{U}/u_\tau$, $y^+ = u_\tau y/\nu$, κ is the von Kármán constant, A is the addictive constant, and the overbar indicates an ensemble average. The logarithmic profile in (1) represents that the only relevant scales in this region are y and u_τ (i.e. $\partial\overline{U}/\partial y \sim u_\tau/y$). At high Reynolds numbers, most of the bulk production and velocity drop originate from the logarithmic layer [1]. Townsend [4] deduced a model for energy-containing eddies in the logarithmic layer whose size scales with y; these structures are *attached* to the wall and self-similar. By assuming that the logarithmic layer consists of the superposition of the attached eddies and that the variation of the Reynolds shear stress across the layer is small compared to the viscous stress, the turbulence intensities ($\overline{u_i^2}$) are expressed as

$$\overline{u^2}^+ = B_1 - A_1 \ln(y/\delta), \tag{1}$$

where A_1 and B_1 are constant. Perry & Chong [5] extended this hypothesis by introducing hiearchies of geometrically similar eddies with the probability distribution function (PDF) that is inversely proportional to their height. Based on this approach, they derived the logarithmic variaion of $\overline{U}$ (1) and $\overline{u^2}$ (2) simultaneously in a sense of the attached-eddy hypothesis. Additionally, they predicted the emergence of a k_x^{-1} (k_x is the streamwise wavenumber) region in the spectrum that is the spectral signature of the attached eddies. In this regard, the attached-eddy hypothesis is a unified theory that links the asympototic behaviors of the turbulence statistics of high-Reynolds-number flows.

Subsequently, several studies [6–8] have refined the model of Perry and Chong [5] to test Townsend's hypothesis, but the Reynolds numbers are not sufficiently high enough to establish the logarithmic region. Recently, advanced measurements confirmed the presence of the k_x^{-1} region [9] and the coexistence of logarithmic regions for $\overline{U}$ and $\overline{u^2}$ at $Re_\tau = O(10^{4\text{-}5})$ [10,11]. However, the central question that has not been resolved is as follows: what is the actual structure in the fully turbulent flow that accords with an attached eddy and forms the logarithmic region? Although Townsend [4] and Perry and Chong [5] proposed a particular shape of eddies based on the flow visualization results, these structures are modeled to formulate the inverse-power-law PDF and the constant shear stress. Additionally, the k_x^{-1} region does not necessarily indicate the attached structure, because one coherent motion can carry the energy with a broad range of wavenumbers [12] and the wavenumber at a given y does not reflect whether that motion is attached to the wall or is part of a detached one [13]. To overcome these limitations, clusters of vortices [14] and three-dimensional sweeps/ejections [15] were identified in direct numerical simulation (DNS) of channel flows. These structures can be classified as either wall-attached or wall-detached. The former are self-similar and statistically dominant structures in the logarithmic layer reminiscent of Townsend's attached eddy, but it has not been shown how these structures contribute to the logarithmic behavior of $\overline{u^2}$.

Here, we show the logarithmic region of $\overline{u^2}$ by identifying the wall-attached clusters of streamwise velocity fluctuations (u) from DNS data of zero-pressure-gradient TBL at $Re_\tau \approx 1000$. We focus on u clusters because long negative-u regions are associated with the net Reynolds shear force [16], and because the outer negative-u structures extend to the wall and interact with the near-wall streaks during the merging of the outer structures [17]. We find that a group of u clusters over a wide range of scales is attached to the wall and self-similar. With these attached clusters, we can reconstruct the streamwise turbulent intensity from the superposition of the identified structures.

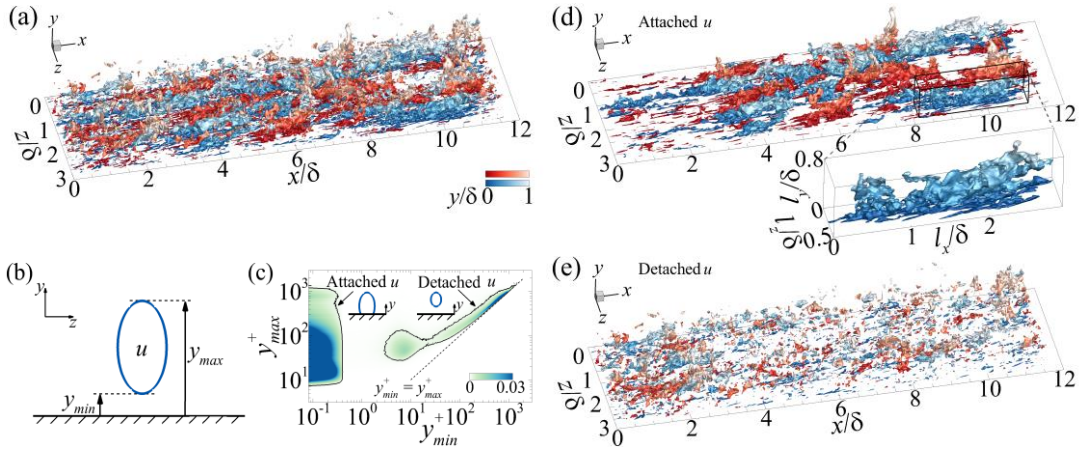

Figure 1. Clusters of streamwise velocity fluctuations (u) in turbulent boundary layer at Re_τ = 980. (a) Isosurfaces of positive- (red) and negative-u clusters (blue) in the instantaneous flow field. Here, the clusters, which cross the edges of the streamwise and spanwise domains, are excluded to represent the size of each cluster completely. (b) Schematic illustration of a u cluster in the cross-stream plane. (c) The number of u clusters per unit wall-parallel area as a function of y_{min} and y_{max}. (d) Isosurfaces of wall-attached structures extracted from (a). (e) Isosurfaces of detached structures extracted from (a).

COMPUTAIONAL DETAILS AND IDENTIFICATION METHOD

The DNS data of the TBL [18] are used in the present study. The DNS was performed using the fractional step method of Kim et al. [19] to solve the Navier–Stokes equations and the continuity equation for the incompressible flow:

$$\frac{\partial U_i}{\partial t}+\frac{\partial}{\partial x_j}U_iU_j=-\frac{\partial P}{\partial x_i}+\frac{1}{\mathrm{Re}_{\delta_0}}\frac{\partial}{\partial x_j}\frac{\partial u_i}{\partial x_j}, \tag{3}$$

$$\frac{\partial U_i}{\partial x_i}=0 \quad (U_i=\overline{U_i}+u_i). \tag{4}$$

Here, all terms are normalized by the inlet boundary layer thickness δ_0 and the free-stream velocity U_∞. The inlet Reynolds number is defined as $\mathrm{Re}_{\delta_0}=U_\infty\delta_0/\nu$. The no-slip boundary condition is applied at the wall, and the top boundary condition is $U=U_\infty$, $\partial V/\partial y=0$, and $W=0$. In the spanwise direction, periodic boundary conditions are imposed. The convective boundary condition is applied at the exit. The inflow condition is set as a superposition of the Blasius velocity profile and the isotropic free-stream turbulence. The free-stream turbulence is generated by the Orr-Sommerfeld and Squire modes in the wall-normal direction and Fourier modes in time and in the spanwise direction [20]. The computational domain is $2{,}300\delta_0 \times 100\delta_0 \times 100\delta_0$ in the streamwise (x), wall-normal (y) and spanwise (z) directions, respectively. Given that the intermittent region appears at the turbulent/non-turbulent interface (TNTI), we define u ($= U-\overline{U}(y,t)$) by considering the height of the local TNTI (δ_i) to minimize the contamination of the fluctuations at the TNTI [21]. This decomposition can precisely detect the tall structures that span δ. The clusters of positive and negative u are the groups of connected points satisfying $|u(\boldsymbol{x})| > \alpha u_{rms}(y, \delta_i)$, where u_{rms} is the root mean square of u and α is the threshold. To characterize the irregular shapes of the u clusters (Fig. 1a), the connectivity of u was defined based on the six orthogonal neighbors of each node in Cartesian coordinates [14,15]. As a result, we could determine the sizes of each cluster with the velocity vectors. The threshold α = 1.5 was chosen based on a percolation transition of the clusters; the results remained qualitatively unchanged within the transition

RESULTS AND DISCUSSION

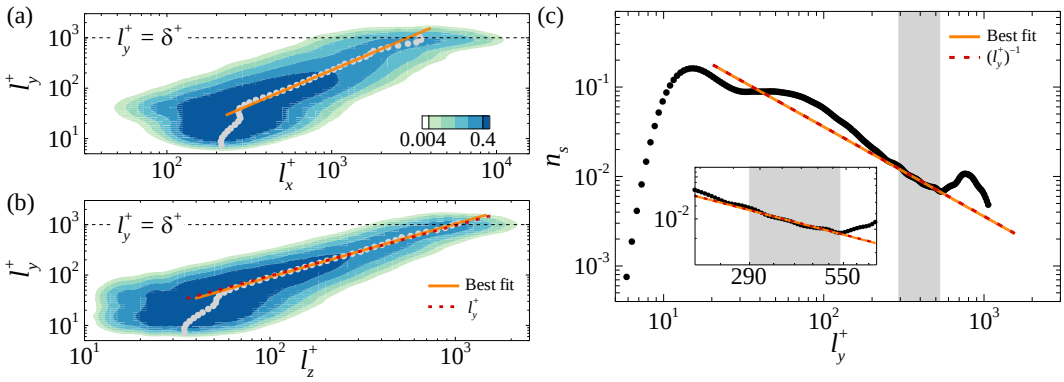

Figure 2. Self-similarity of attached structures and their population density. (a,b) Joint PDFs of the logarithms of the sizes (l_x and l_z) of the attached structures and of the height (l_y). The inserted dots indicate the mean l_x and l_z with respect to l_y. (a) The solid line is the best fit, $l_x^+ \sim (l_y^+)^{\gamma 1}$ with $\gamma_1 = 0.745$ of the data for $100 < l_y^+ < 550$. (b) The dashed line is $l_z^+ = 1.04 l_y^+$ and the solid line is the best fit, $l_z^+ \sim (l_y^+)^{\gamma 2}$ with $\gamma_2 = 0.949$ of the data for $l_y^+ > 100$. The contour levels are logarithmically distributed. (c) Population density of the attached clusters (n_s) with respect to their height l_y. The dashed line is $n_s \sim (l_y^+)^{-1}$ and the solid line is the best fit, $n_s \sim (l_y^+)^{\beta}$ with $\beta = -1.001$ of the data for $290 < l_y^+ < 550$.

The population density of clusters according to their minimum and maximum y (y_{min} and y_{max}) shows two distinct regions (figure. 1c), yielding that the clusters are classified into two groups; wall-attached structures with $y_{min} \approx 0$ (figure 1d) and detached structures with $y_{min} > 0$ (figure 1e). The height of the attached structures ($l_y \approx y_{max}$) varies from the near-wall region to δ and they contribute 64% of the total volume of the clusters. Moreover, these attached structures are geometrically self-similar. The distributions of their length (l_x) and width (l_z) with respect to l_y (figure 2a,b) show two distinct growth rates. For the buffer-layer structures ($l_y^+ < 60$), l_x and l_z increase gradually whereas those of the taller structures ($l_y^+ > 100$) grow rapidly until l_y is bounded by δ. For $l_y^+ > 100$, the mean l_x and l_z (circles) scale with l_y, representing a strong tendency for the self-similarity over a broad range, although there is some dispersion at a given l_y. Since the mean l_x and l_z indicate the sizes of representative structures, the dispersion would be associated with hierarchies at different stages of stretching [5]. The mean l_z especially follows a linear law $l_z^+ \approx l_y^+$, indicating that the spanwise length scale of the structures is proportional to the distance from the wall.

The population density of the attached u structures versus l_y is examined to determine whether the attached structures are associated with the hierarchy length scales [5,6]. In figure 2(c), the distribution decays with l_y beyond the buffer layer, and in particular, it is inversely proportional to l_y for $290 < l_y^+ < 550$ (shaded region). Given the inverse-power-law PDF of hierarchy scales [5], the structures in the shaded region are hierarchies of self-similar eddies. Furthermore, a peak is evident at $l_y^+ \approx 800$, indicating the additional weighting for the large-scale structures. In other words, these large-scale structures are not geometrically self-similar in connection with the protrusions around $l_y^+ = \delta^+$ in figure 2(a,b). This behavior is consistent with the modified PDF of hierarchy scales [6], which was proposed to enable the more accurate prediction of the mean velocity defect and energy spectra.

The question then arises: do these attached structures actually form the logarithmic variation of $\overline{u^2}$? To answer this question, the streamwise turbulence intensity carried by attached structures with different heights $\overline{u_a^2(y,l_y)}$ is defined as

$$\overline{u_a^2(y,l_y)} = \left\langle \frac{1}{S_a(y,l_y)} \oint_{S_a} u(\boldsymbol{x}) u(\boldsymbol{x}) dxdz \right\rangle, \qquad (3)$$

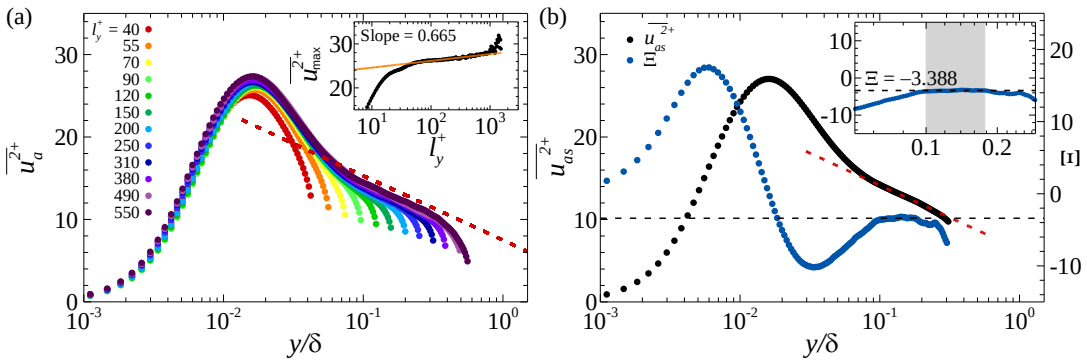

Figure 3. Logarithmic behavior of the streamwise turbulence intensity carried by attached structures. (a) Wall-normal variations of the streamwise turbulence intensity ($\overline{u_a^2}$) within the attached structures of u for various l_y. The dashed line corresponding to the logarithmic variation is a guide for the eye. (b) Superposition of $\overline{u_a^2}$ carried by the attached structures with a population density that is inversely proportional to their height ($290 < l_y^+ < 550$ in figure 2b), $\overline{u_{as}^2}$. The blue dot indicates $\Xi = y\partial\overline{u_a^2}^+/\partial y$, which is the indicator function of the logarithmic law.

where S_a is the wall-parallel area of the structures with l_y at a given y and the angle brackets denote an ensemble average. In figure 3(a), the logarithmic region arises at $l_y^+ > 120$ and this region extends with increasing l_y. Although the magnitude of $\overline{u_a^2}$ is larger than that of $\overline{u^2}$ because the extracted structures are defined as $|u| > 1.5u_{rms}$, this result is remarkable considering the Reynolds number of the present TBL ($Re_\tau = 980$); the logarithmic behavior of $\overline{u^2}$ was observed at $Re_\tau = O(10^{4\text{-}5})$ in experiments [10,11]. In addition, the superposition of $\overline{u_a^2}$ ($\overline{u_{as}^2}$) over $290 < l_y^+ < 550$ is presented in figure 3(b). Here, $\overline{u_{as}^2}$ was computed by weighting the relative probability of the structures to the corresponding $\overline{u_a^2}$. To confirm the logarithmic variation of $\overline{u_{as}^2}$, the indicator function $y\partial\overline{u_{as}^2}^+/\partial y$, which is constant in the logarithmic region, is also plotted. A plateau appears in $100 < y^+ < 0.18\delta^+$, verifying the presence of the logarithmic region formed by the attached structures.

CONCLUSIONS

We have demonstrated for the first time that the wall-attached structures of u are energy-containing motions satisfying the attached-eddy hypothesis [4], not only because they are self-similar to l_y, but also because there are two strong pieces of evidence: (i) the inverse-power-law PDF, and (ii) the logarithmic variation of $\overline{u^2}$. In particular, we show the presence of the logarithmic region by reconstructing from the superposition of the wall-attached structures in spite of the absence of the logarithmic behavior in the total $\overline{u^2}$. Although we identified the attached structures in a TBL for a single Reynolds number, their hierarchical features will ensure their presence in high-Reynolds-number flows. We anticipate that examining the Reynolds-number effects on attached structures will improve the predictive model [22] and exploring their dynamics will facilitate deeper insights into the multiscale energy cascade of wall turbulence.

ACKNOWLEDGEMENTS

This work was supported by the National Research Foundation of Korea (No. 2018001483), and partially supported by the Supercomputing Center (KISTI).

REFERENCES

1. A. J. Smits, B. J. McKeon and I. Marusic, Annu. Rev. Fluid Mech. **43**, 353 (2011).
2. S. K. Robinson, Annu. Rev. Fluid Mech. **23**, 601 (1991).
3. C. M. Millikan, in *Proc. 5th Int. Congress for Appl. Mech*. (Wiley, 1938), p. 386.
4. A. A. Townsend, *The structure of turbulent shear flow* (Cambridge University Press, Cambridge, 1976), Vol. 2.
5. A. E. Perry and M. S. Chong, J. Fluid Mech. **119**, 163 (1982).
6. A. E. Perry, S. M. Henbest, and M. S. Chong, J. Fluid Mech. **165**, 163 (1986).
7. A. E. Perry, and I. Marusic, J. Fluid Mech. **298**, 361 (1995).
8. I. Marusic, and G. J. Kunkel, Phys. Fluids **15**, 2461 (2003).
9. T. B. Nickels *et al*., Phys. Rev. Lett. **95**, 074501 (2005).
10. M. Hultmark *et al*., Phys. Rev. Lett. **108**, 094501 (2012).
11. I. Marusic *et al*., J. Fluid Mech. **716**, R3 (2013).
12. T. B. Nickels, and I. Marusic, J. Fluid Mech. **448**, 367 (2001).
13. J. Jiménez, Phys. Fluids **25**, 101302 (2013).
14. J. C. del Álamo *et al*., J. Fluid Mech. **561**, 329 (2006).
15. A. Lozano-Durán, O. Flores, and J. Jiménez, J. Fluid Mech. **694**, 100 (2012).
16. J. Hwang, J. Lee, and H. J. Sung, J. Fluid Mech. **804**, 420 (2016).
17. J. Hwang, *et al*., J. Fluid Mech. **790**, 128 (2016).
18. J. Hwang, and H. J. Sung, J. Fluid Mech. **829**, 751 (2017).
19. K. Kim, S. J. Baek, and H. J. Sung, Intl J. Number. Meth. Fluids **38**, 125 (2002).
20. R. G. Jacobs and P. A. Durbin, J. Fluid Mech. **428**, 185 (2001)
21. Y. S. Kwon, N. Hutchins, and J. P. Monty, J. Fluid Mech. **794**, 5 (2016).
22. I. Marusic, R. Mathis, and N. Hutchins, Science **329**, 193 (2010).